Heterodyne Common-Path Interference Microscope with a Wavelength-Tunable Diode Source

Shunpei Yukita[1], Yukihiro Ishii[1,2], Kosuke Kiyohara[2],
Jun Chen[3], and Eiji Tokunaga[1]

[1] Tokyo University of Science, 1-3 Kagurazaka, Shinjuku-ku, Tokyo 162-8601, Japan
shunpei.yukita@gmail.com
[2] Kiyohara Optics Inc. , 6-23-2 Shinjuku, Shinjuku-ku, Tokyo 162-0022, Japan
[3] Tokyo Polytechnic University, 1583 Iiyama, Atsugi 243-0297, Japan

1 Introduction

The temporal carrier beat frequencies in an optical heterodyne interferometer can be generated by ramping the wavelength in a laser diode (LD) based on the frequency-modulated continuous-wave (FMCW) techniques [1,2]. The beat frequency is proportional to the optical path difference (OPD) of each pair of interfering beams in an interferometer [3]. It enables us to construct an optical heterodyne interferometer on an unbalanced OPD without auxiliary frequency modulators. Multiple-beam interferometry can produce the different beat frequencies by using a wavelength-tunable LD [4]. An LD interferometer has been applied to 3-D imaging by using the optical frequency domain reflectometry [5]. A technique of a holographic radar has been applied to measure the range information with a frequency-tunable laser [6]. 3-D object can be holographically reconstructed by the electronic tuning with beat signals by a current-modulated LD [7]. A phase-shifting common-path interferometer has been demonstrated with a biprism beam splitter [8].

We demonstrate a new type of optical heterodyne common-path interferometer with a birefringent beam splitter with a wavelength-tunable external-cavity laser-diode (ECLD) source. A Wollaston prism is employed in an interferometer as a birefringent beam splitter [9]. A two-dimensional (2-D) phase map of a phase object in transmission can be derived from the numerical Fourier transformation of measured heterodyne interference fringes. Precise measurements are shown because the common-path interferometer [10] is quite insensitive to external disturbances.

W. Osten (ed.), *Fringe 2013*,
DOI: 10.1007/978-3-642-36359-7_148,

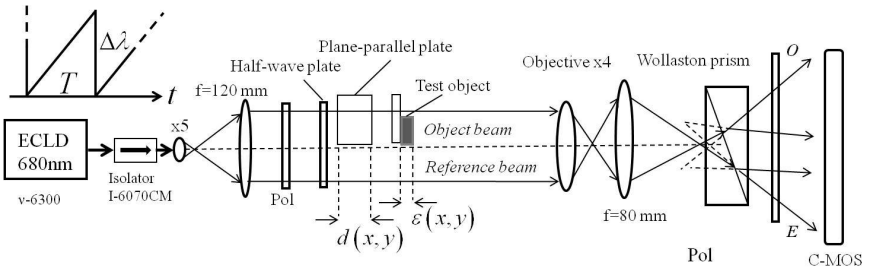

Fig. 1 Setup of a heterodyne common-path interferometer

2 Optical Heterodyne Common-Path Interferometer

A setup of a common-path interferometer is shown in Fig. 1 with a plane-parallel plate with a thickness d giving an unbalanced OPD. A light source is a wavelength-tunable ECLD (ν-focus, ν-6300) those widely tuned wavelength diversity in the experiment is $\Delta\lambda$=~2 nm at a central wavelength of λ=680 nm. A collimated beam from an ECLD has an upper object beam with a phase object in transmission adding with an unbalanced OPD $2\pi nd/\lambda$ where n is index of a plane-parallel glass. An ITO (indium tin oxide) thin film is put on an object beam as a phase object of the thickness variation $\varepsilon(x,y)$ of an index n_i. A lower beam is a reference wave. Both object and reference waves are magnified with a microscope objective plus a convex lens and imaged onto a CMOS camera with a 7× lateral magnification. Both beams are incident on a Wollaston prism through a half-wave plate of a 45°-azimuth polarization that splits into *O* and *E* rays travelling in different direction. Both waves are laterally sheared and are interfered with each other after passing through a polarizer. Half divergent angle on a front face of a Wollaston prism is adjusted to be almost equal to a splitting angle of a prism. A splitting angle θ is 2° at 633 nm that forms the Young fringes of low spatial frequency. It makes it possible for resolving the fringe pattern by using a CMOS camera. They pass through the common optical path; consequently the interferometer is rather insensitive to the vibration in which the improved measurement accuracy has been assured.

Complex amplitudes $u_o(x_c,y_c)$ and $u_r(x_c,y_c)$ of object and reference beams are

$$\begin{aligned} u_o(x_c,y_c)&=\exp[ik\{nd+ns+n_i\varepsilon(x_c,y_c)\}] \\ u_r(x_c,y_c)&=\exp[ik\{\ \ d+\ \ s+\ \ \ \varepsilon(x_c,y_c)\}] \end{aligned} \tag{1}$$

where k is the wavenumber, (x_c, y_c) is the coordinate of CMOS imaging plane, and s is the thickness of a slide glass evaporating with an ITO thin film.

A Wollaston prism can generate two virtual point sources by birefringent refraction that form the Young fringes. The angle extending two point sources is

approximately equal to half a splitting angle of Wollaston prism. The unit complex amplitudes U_{or} and U_{ex} of *O* and *E* waves are given by

$$\begin{aligned} U_{or}(x_c, y_c) &= \exp[i\frac{2\pi n_0}{\lambda}\{x_c \sin(\frac{\theta}{2}) + z\cos(\frac{\theta}{2})\}] \\ U_{ex}(x_c, y_c) &= \exp[i\frac{2\pi n_e}{\lambda}\{x_c \sin(-\frac{\theta}{2}) + z\cos(\frac{\theta}{2})\}] \end{aligned} \tag{2}$$

where n_o and n_e are indices of ordinary and extraordinary rays, respectively. An interference intensity $I(x_c, y_c)$ is given by a squared absolute value of the summed interference beams, i.e.,

$$\begin{aligned} &I(x_c, y_c) = \left|u_o U_{ex} + u_r U_{or}\right|^2 \propto (u_o U_{ex} u_r^* U_{or}^* + u_o^* U_{ex}^* u_r U_{or}) \\ &\approx 2\cos[\frac{2\pi}{\lambda}[\{(n_i\text{-}1)\varepsilon(x_c, y_c) + (n\text{-}1)(d+s)\}\text{-}\{(n_e + n_o)(x_c \sin\tfrac{\theta}{2})\}]] \end{aligned} \tag{3}$$

by using Eqs. (1) and (2) where the asterisk symbol * shows the complex conjugate. Here it is assumed that the negative birefringence $\Delta n = n_e - n_0$ of a Wollaston calcite prism is very small than the average index of prism, and $(d+s) \gg \varepsilon$. Two parabolic phases divergent from two virtual points interfere each other, and then are cancelled because of very small birefringence Δn.

When the wavelength of ECLD linearly changes by $\Delta\lambda$ as shown in an upper left of Fig. 1 with the modulation frequency $f_s(=1/T)$, the interference beat signal $i(x_c, y_c; t)$ of frequency f_b is generated between object and reference beams, giving

$$\begin{aligned} &i(x_c, y_c; t) \propto 2\cos[\frac{2\pi}{\lambda}[\{(n_i\text{-}1)\varepsilon(x_c, y_c) + (n\text{-}1)(d+s)\} \\ &\text{-}\{(n_e + n_o)(x_c \sin\tfrac{\theta}{2})\}] - 2\pi f_b t] \end{aligned} \tag{4}$$

from Eq. (3) where the beat frequency is $f_b \cong (n_g\text{-}1)(d+s)\Delta\lambda/(\lambda^2 T)$ with a group index n_g almost equaling to an index n due to small wavelength diversity. The term $k(n_e + n_o)(x_c \sin\frac{\theta}{2})$ is expressed by the spatial carrier fringes, i.e., Young fringes. At an appropriate coordinate x_c of an image sensor, the Fourier transformation of the heterodyne interference signal in Eq. (4) gives the phase,

$$\Im[i(x_c, y_c; t)] \propto \exp[i\frac{2\pi}{\lambda}\{(n_i\text{-}1)\varepsilon(x_c, y_c) + (n\text{-}1)(d+s)\}]\delta(f\text{-}f_b) \tag{5}$$

where $\Im[...]$ represents the Fourier transform and $\delta(\ldots)$ is delta function. By using Eq. (5) and subtracting constant phase from it, 2-D phase distribution $2\pi(n_i\text{-}1)\varepsilon(x_c, y_c)/\lambda$ can be measured from heterodyne interference patterns in Eq. (4)

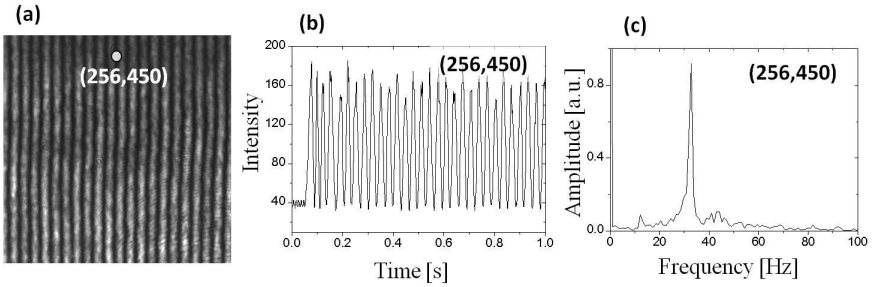

Fig. 2 Interference pattern (a), heterodyne signal (b) and power spectrum (c)

3 Results

On the measurement, the square wave from an electronic function generator is triggered to two inputs of both ECLD diode source and high-speed CMOS camera (Redlake, HS-3). Then the wavelength emitted by ECLD starts to scan and 2-D heterodyne interference pattern is simultaneously captured by CMOS camera that is sent to a computer with 512×512 samples of 8-bit level. Fig. 2 shows a magnified 2-D fringe patttern (a) forming rectilinear fringes of an ITO thin film to be tested, a heterodyne beat signal (b) at (256, 450) pixel, and its power spectrum (c) by calculation in a beat frequency f_b=32 Hz. Fringe signal has high visibility with less noise. When the beat frequency f_b differs from the modulation frequency f_s, some systematic phase error is occured [11]. Nevertheless when the beat frequency f_b is enough higher than the modulation frequncy f_s in Fig. 2(b), the phase error becomes negligible.

Phase gradient of ITO film can be measured with an addtional phase measurement in which the ITO thin film is removed on an object arm. Figs. 3 (a) and (c) show the wrapped phase map (a) and the unwrapped phase map (c) in grey demonstration exhibiting the phase k(n-1)d. Figs. 3 (b) and (d) show the wrapped phase map (b) and the unwrapped phase map (d) in grey demonstration in which the ITO thin film is inserted into an object arm exhibiting the phase $k\{(n_i-1)\varepsilon+(n-1)(d+s)\}$ in Eq. (5). The subtraction of the phase in Fig. 3 (c) from the phase in Fig. 3 (d) gives the phase $k\{(n_i-1)\varepsilon+(n-1)s\}$ of ITO thin film shown in Figs. 3 (e) in grey demonstration and (f) in 3-D phase map. The small phase step of ~2.2 rad (=~λ/3) in Fig. 3 (f) can be measured.

Fig. 4 shows the cross-sectional phases at x_c=260 pixel extracted from 2-D phase map in Fig. 3 (e) under the phase-difference procedure. Two phases are presented in solid and dashed lines in Fig. 4 those phase difference shown in the dotted line exhibits the rms phase value of ~0.01 rad(=~λ/630) by averaging the phases with 512 pixels. Two phases coincide with each other so that stable phase measurement can be assured because of common-path interferometric capability.

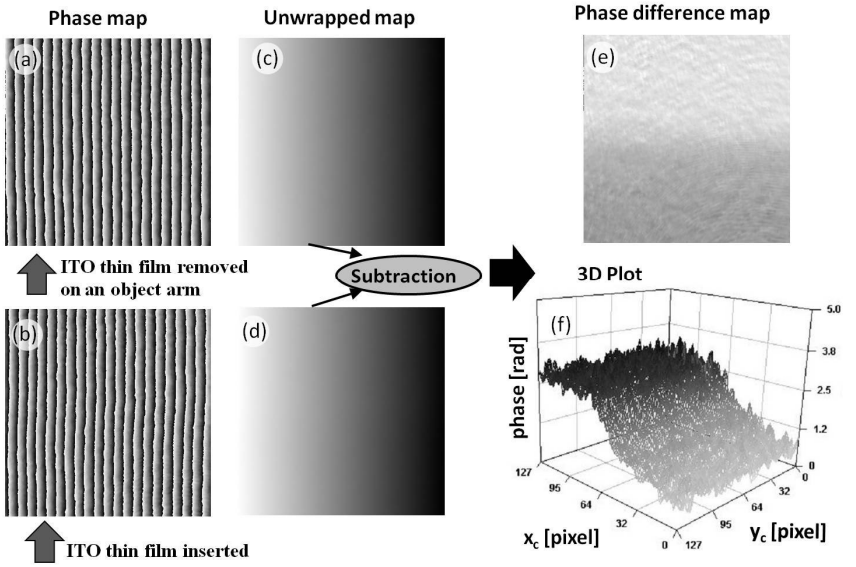

Fig. 3 Subtraction of unwrapped phase (c) of the object film removed from unwrapped phase (d) of the object inserted gives the measured phase difference of ITO film in (e) and (f)

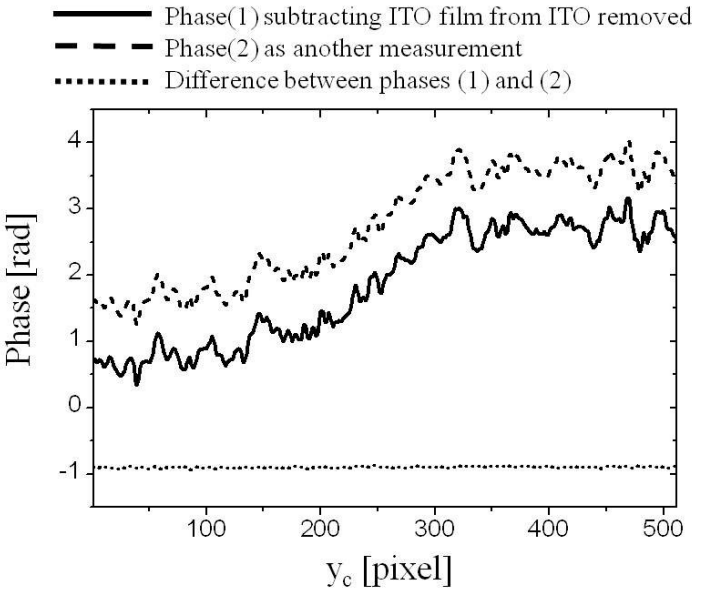

Fig. 4 Two cross-sectional phases extracted from two measurements are shown in solid and dashed curves. Two phases in dotted line agree.

4 Conclusions

A newly developed heterodyne common-path interferometer with a Wollaston birefringent beam splitter acts to eliminate the external disturbances, assuring that precise phase measurement is performed. The optical heterodyne signals can be generated by a wavelength-tunable external-cavity laser-diode source.

References

1. Giles, I.P., Uttam, D., Culshaw, B., Davies, D.E.N.: Coherent optical-fibre sensors with modulated laser sources. Elect. Lett. 19, 395–396 (1983)
2. Zheng, J.: Optical frequency-modulated continuous-wave (FMCW) interferometry. Springer (2005)
3. Ishii, Y.: Laser-diode interferometry. In: Wolf, E. (ed.) Prog. Opt., vol. 46, pp. 243–309. Elsevier (2004)
4. Suematsu, M., Takeda, M.: Wavelength-shift interferometry for distance measurements using the Fourier transform technique for fringe analysis. Appl. Opt. 30, 4046–4055 (1991)
5. Yoshimura, T., Masazumi, N., Shigematsu, Y.: Imaging a reflecting plate located in scattering media using optical frequency domain reflectometry. Opt. Rev. 4, 227–227 (1997)
6. Marron, J.C., Schroeder, K.S.: Holographic laser radar. Opt. Lett. 18, 385–387 (1993)
7. Onodera, R., Ishii, Y.: Multiplex imaging by a frequency-ramped laser-diode interferometer. Opt. Commun. 149, 143–151 (1998)
8. Endo, J., Chen, J., Kobayashi, D., Wada, Y., Fujita, H.: Transmission laser microscope using the phase-shifting technique and its application to measurement of optical waveguides. Appl. Opt. 41, 1308–1314 (2002)
9. Françon, M.: Polarization, Modern applications of physical optics, pp. 91–103. John Wiley and Sons (1963)
10. Mallick, S., Malacara, D.: Common-path interferometer. In: Malacara, D. (ed.) Optical Shop Testing, 3rd edn., pp. 97–118. John Wiley and Sons (2007)
11. Onodera, R., Ishii, Y.: Effect of beat frequency on measured phase of laser-diode heterodyne interferometry. Appl. Opt. 35, 4355–4360 (1996)